Supporting Information

Customized CO_2 electroreduction to methane or ethylene by manipulating *H and *CO adsorption on Cu/CeO_x catalysts

T. H. Yang, Y. B. Zhang, Z. C. Huang, Prof. J. P. Yang, Prof. M. Kuang

State Key Laboratory for Modification of Chemical Fibers and Polymer Materials, College of Materials Science and Engineering, Donghua University, Shanghai 201620, China

E-mail: jianpingyang@dhu.edu.cn, mkuang@dhu.edu.cn

Chemicals and Materials

The chemical reagents and suppliers used in this article are listed as follows. HCl was purchased from Sinopharm Chemical Reagent Co., LTD. CuCl was purchased from Shanghai Aladdin Biochemical Technology Co., Ltd. $Ce(NO_3)_3 \cdot 6H_2O$ and NaOH were purchased from Shanghai Macklin Biochemical Co., Ltd. Deionized water (18.2 MΩ cm^{-2}) was used in this work. No further purification is required when all reagents are used.

Synthesis of $Cu/CuCeO_x$ nanorods

The $Cu/CuCeO_x$ nanorods catalysts are prepared according to the previously reported co-precipitation method.[1] Firstly, a certain amount of CuCl was dissolved in 5 mL concentrated hydrochloric acid, then 8 mmol $Ce(NO_3)_3 \cdot 6H_2O$ was added into the solution, and the mixture solution was stirring magnetically until it is fully dissolved to form a dark green solution. At the same time, 140 mL of NaOH solution (38.4 g) was prepared. After cooled to room temperature, the NaOH solution was added to the hydrochloric acid solution of CuCl and $Ce(NO_3)_3 \cdot 6H_2O$ under vigorous stirring, followed by continuous stirring for 30 min to form a brownish yellow suspension. The above steps are carried out under the protection of a nitrogen atmosphere at 30 ℃. After the reaction, the suspension was centrifuged, washed alternately with ethanol and deionized water to neutral, dried at 60 ℃ overnight and then calcined at 500 ℃ for 2 h. The obtained $Cu/CuCeO_{2-x}$ nanorods with different copper mass content of 10%, 30% and 50% (the content percentage means the mass percentage of Cu/(Cu+Ce)) were marked as $Cu_{0.1}/CuCeO_x$, $Cu_{0.3}/CuCeO_x$, and

$Cu_{0.5}/CuCeO_x$, respectively. In addition, pure CeO_x and Cu was prepared as a control sample according to the above process without CuCl or $Ce(NO_3)_3 \cdot 6H_2O$.

Synthesis of Cu/CeO_x nanorods

Based on the synthesis of CeO_x, we used the impregnation method by controlling the copper precursor amount to obtain different ratios of Cu/CeO_x. Different ratios of copper precursor salt and 200 mg of cerium dioxide were dispersed in 100 mL of ultrapure water to obtain a homogeneous mixed solution. After standing for 12 hours, it is washed alternately with water and ethanol, dried and calcined, etc.

Characterizations

Transmission electron microscope (TEM) images of the as-synthesized $Cu/CuCeO_x$ and Cu/CeO_x were acquired using JEM-2100 (operated at 200 kV). High-angle annular dark-field scanning transmission electron microscopy (HAADF-STEM) and elemental mapping analysis were performed on Talos F200S operated at 200 kV. XRD was carried out on D8 Advance in the 2θ range from 10° to 90°. H nuclear magnetic resonance (NMR) spectra were collected on Bruker AVANCE III 600 MHz nuclear magnetic resonance spectrometer. The elemental valences of $Cu/CuCeO_{2-x}$ were taken on X-ray photoelectron spectrometry (XPS) (Thermo Scientific, ESCALAB 250Xi, Mg X-ray source). The actual Cu loading of prepared catalysts were obtained by an inductively coupled plasma atomic emission spectroscopy (ICP-OES) on Leeman Prodigy. The Raman spectra were obtained with Dilor LabRam-1B microscope Raman spectrometer (France).

Electrochemical measurements

The electrocatalytic performance of $Cu/CuCeO_x$ toward the CO_2RR was evaluated in a flow-cell with 1.0 M KOH solution as the electrolyte, and equipped with a gas diffusion electrode (GDE). The cathode and anode were separated by an anion exchange membrane. GDE was the working electrode, Ni foam was the counter electrode, and Ag/AgCl was the reference electrode in all measurements. Before the electrochemical testing, cyclic voltammetry (CV) measurements were conducted in 1.0 M KOH electrolyte, over a potential range of -1.0 to -2.7 V_{RHE} with a sweep rate of 100 mV S^{-1}, for a total of 5 cycles. Subsequently, linear scanning voltammetry (LSV) was also performed on the catalysts. To prepare the catalyst ink, 8 mg of the catalyst and 2 mg conductive black was dispersed in a mixture of 2 mL acetone and 80 μL Nafion solution. The mixture was then ultrasonicated for 45 min to obtain a homogenous catalyst ink. Subsequently, the catalyst ink was carefully loaded onto the surface of gas diffusion electrode (1×3 cm^2) using a micropipette (pipette) and dried under ambient conditions. The amount of the catalyst on the electrode was 0.5 mg cm^{-2}.

CO_2 reduction products analysis

The gas product was analyzed by an on-line gas chromatography (GC 2060) equipped with flame ionization detector (FID) and thermal conductivity detector (TCD), and using argon (Ar) as the carrier gas. From the standard curves of FID and TCD and the peak areas of the GC, the molar amounts of the gaseous products can be calculated. And the FE of gas

products was calculated as shown in equation (2).

$$FE = \frac{Q_g}{Q_{total}} \times 100\% = \frac{\frac{v}{60\ s\ min^{-1}} \times \frac{y}{24.5\ L\ mol^{-1}} \times n \times F}{j_{average}} \times 100\%$$

(2)

Where v is the flow rate of CO_2 gas, which is controlled by the gas flowmeter at 40 sccm； y is the volume percentage of the target component in the tail gas obtained by the GC 2060; n is the number of electron transfers required for the conversion of CO_2 to the target product. For the gas phase reduction products H_2, CO, CH_4 and C_2H_4, n is 2, 2, 8 and 12, respectively; F (96485 C mol^{-1}) is Faradaic constant; $j_{average}$ is the average current.

The quantification of liquid products was collected using a nuclear magnetic resonance (NMR) spectrometer (Bruker AVANCE III 600 MHz) in D_2O (deuterated water) with dimethyl sulfoxide (DMSO) as the internal standard. The moles of the liquid product were determined based on the integral areas obtained from NMR spectra and calibration curves. Equation (3) is used to calculate the Faraday efficiency of the liquid phase product.

$$FE = \frac{n\ c\ V\ F}{Q} \times 100\% \quad (3)$$

n is the number of electron transfers required for the conversion of CO_2 to the target product. For the gas phase reduction products HCOOH, CH_3COOH and C_2H_5OH, n is 2, 8 and 12, respectively; c is the concentration of a liquid product; V is the volume of electrolytic liquid; F (96485 C mol^{-1}) is Faradaic constant; and Q is the amount of charge.

In Situ FTIR testing

In-situ FTIR measurement was performed at Thermo IS 50. A sample greater than 10 mg was prepared as a catalyst ink and drop-coated on the silicon crystal. The other conditions were the same as the CO_2 electroreduction performance test. The spectra were collected along with negative-going linear sweep voltammetry (LSV) to -1.8 V_{RHE} at a scan rate of 5 mV/s in the scanning range of 1000-3000 cm^{-1}.

In Situ Raman testing

In-situ Raman measurement was performed at Horiba Jobin Yvon HR evolution system, with air-cooled light source of 532 nm. In situ Raman experiment was performed at a potential of -0.6 V to -1.6 V_{RHE}, and 1.0 M KOH aqueous solution was circulated in the cathode cavity through a peristaltic pump while the CO_2 flow rate was maintained at 20 sccm by a mass flow controller.

Computational details

All the density functional theory calculations presented in this paper are performed based on the Vienna Ab-initio Simulation Package (VASP)[2, 3] with the projected augmented wave (PAW) plane-wave method.[4] The electron exchange correlation energy is described using the Perdew-Burke-Ernzerhof (PBE) functional in the generalized gradient approximation (GGA).[5] The cutoff energy was set at 450 eV, and Monkhorst Pack k-point grids of 2 × 2 × 1 meshes were used for the surface. To avoid the effects of periodic image interactions, a 15 Å vacuum layer was added in the Z direction. Structural relaxation stops

until the required self-consistency accuracy of 10^{-5} eV and force of 0.02 eV $Å^{-1}$ were achieved. For catalyst relaxation, the top three layers of CeO_2 substrate were relaxed and the bottom three layers were fixed.

Supplementary Figures

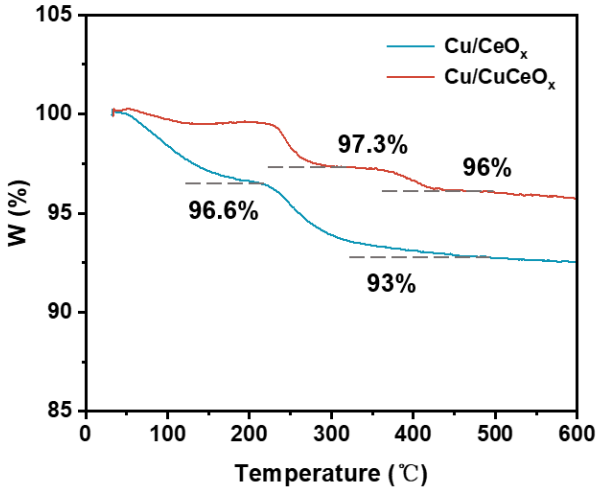

Figure S1 The thermogravimetric analysis of Cu/CuCeO$_x$ and Cu/CeO$_x$.

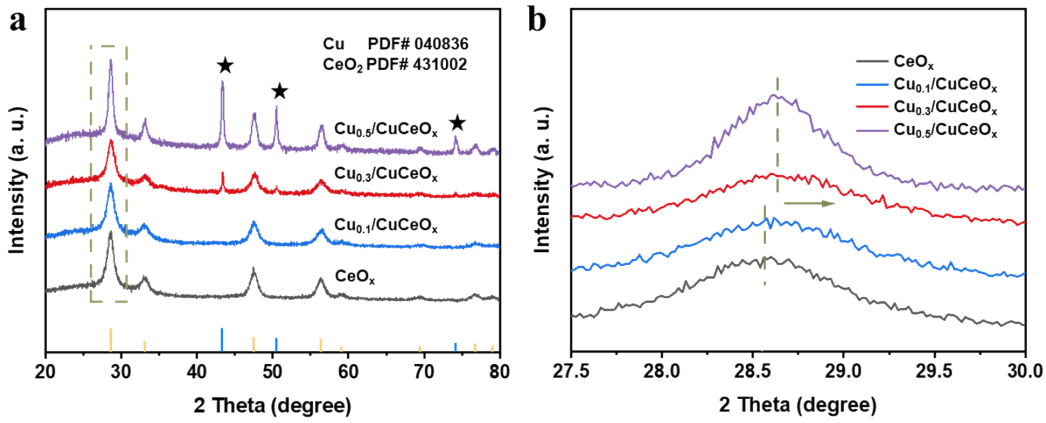

Figure S2 XRD spectra and layout magnification of $Cu_y/CuCeO_x$.

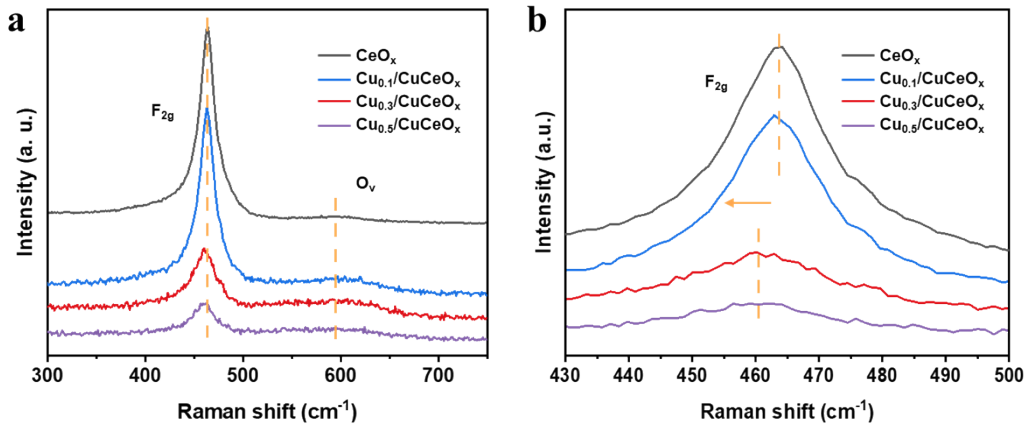

Figure S3 Raman spectra and layout magnification of of $Cu_y/CuCeO_x$.

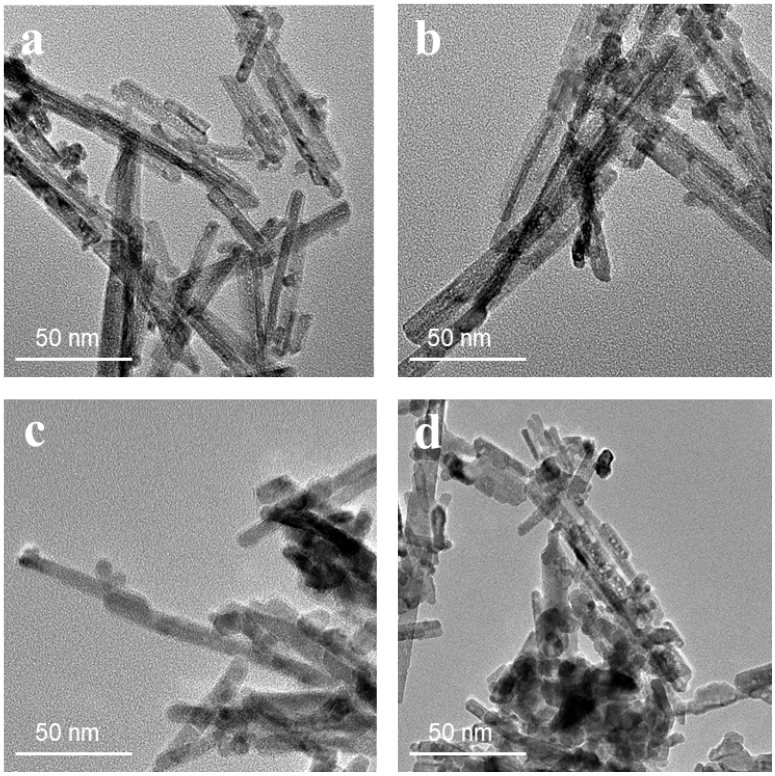

Figure S4 TEM images of (a) CeO_x, (b) $Cu_{0.1}/CuCeO_x$, (c) $Cu/CuCeO_x$, and (d) $Cu_{0.5}/CuCeO_x$ nanorods.

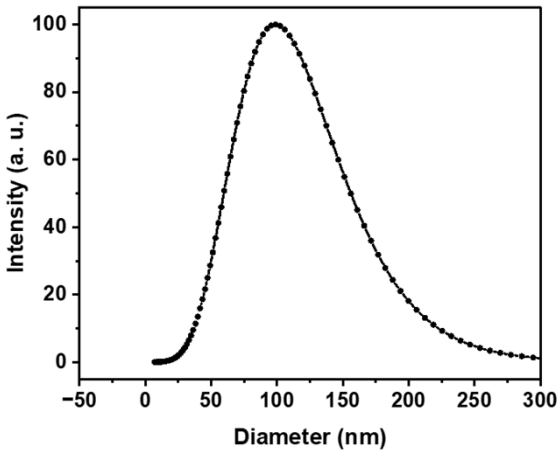

Figure S5 The dynamic light scattering of CeO_2.

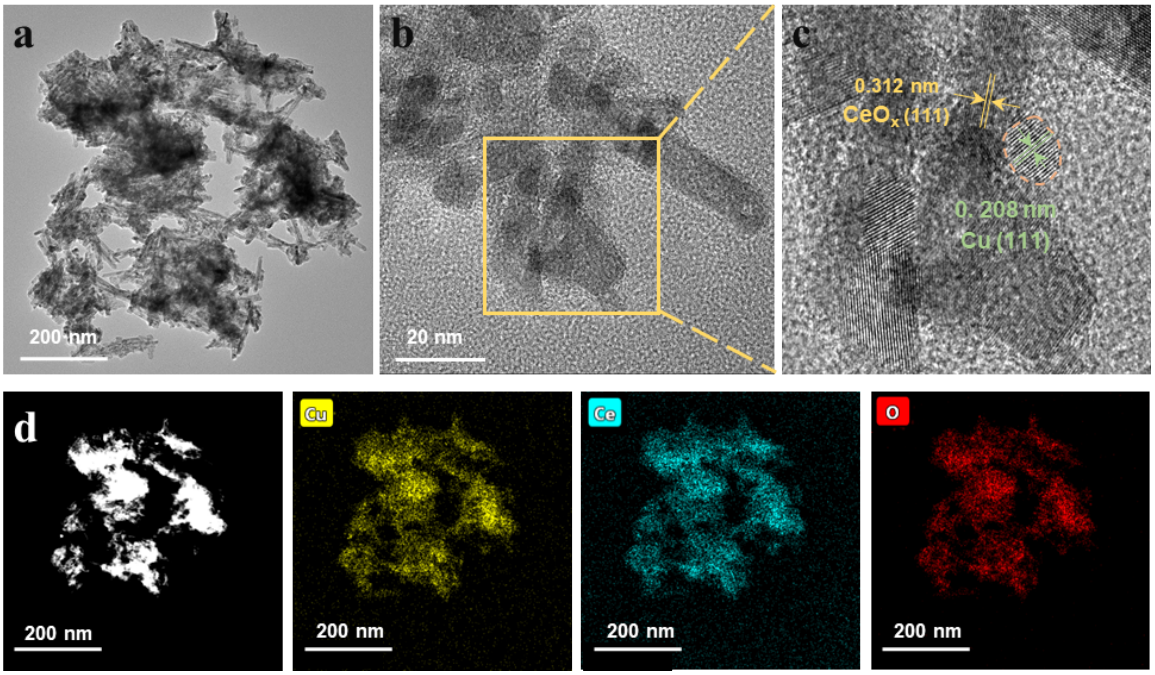

Figure S6 (a-c) HRTEM images of Cu/CeO_x nanorods by impregnation method. (d) EDX elemental distribution mapping images of Cu/CeO_x nanorods.

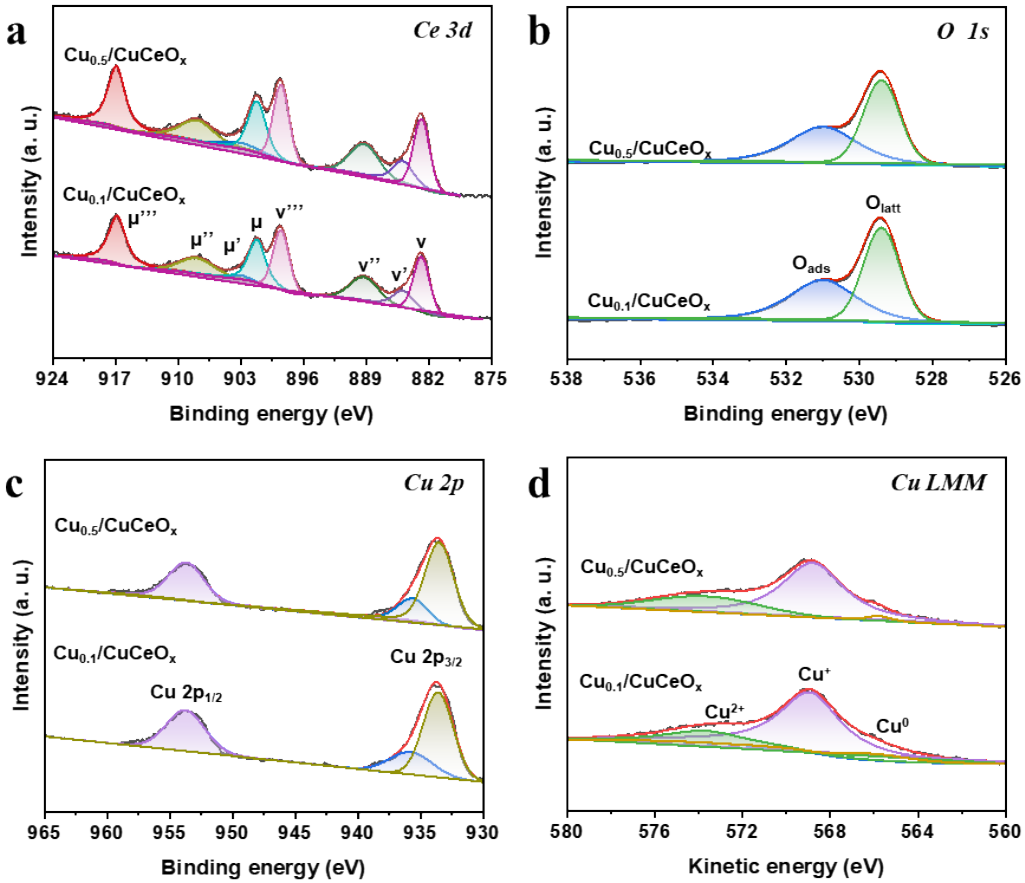

Figure S7 XPS analysis of (a) Ce 3d, (b) O1s, (c) Cu 2p and (d) Cu LMM for $Cu_{0.1}/CuCeO_x$ and $Cu_{0.5}/CuCeO_x$.

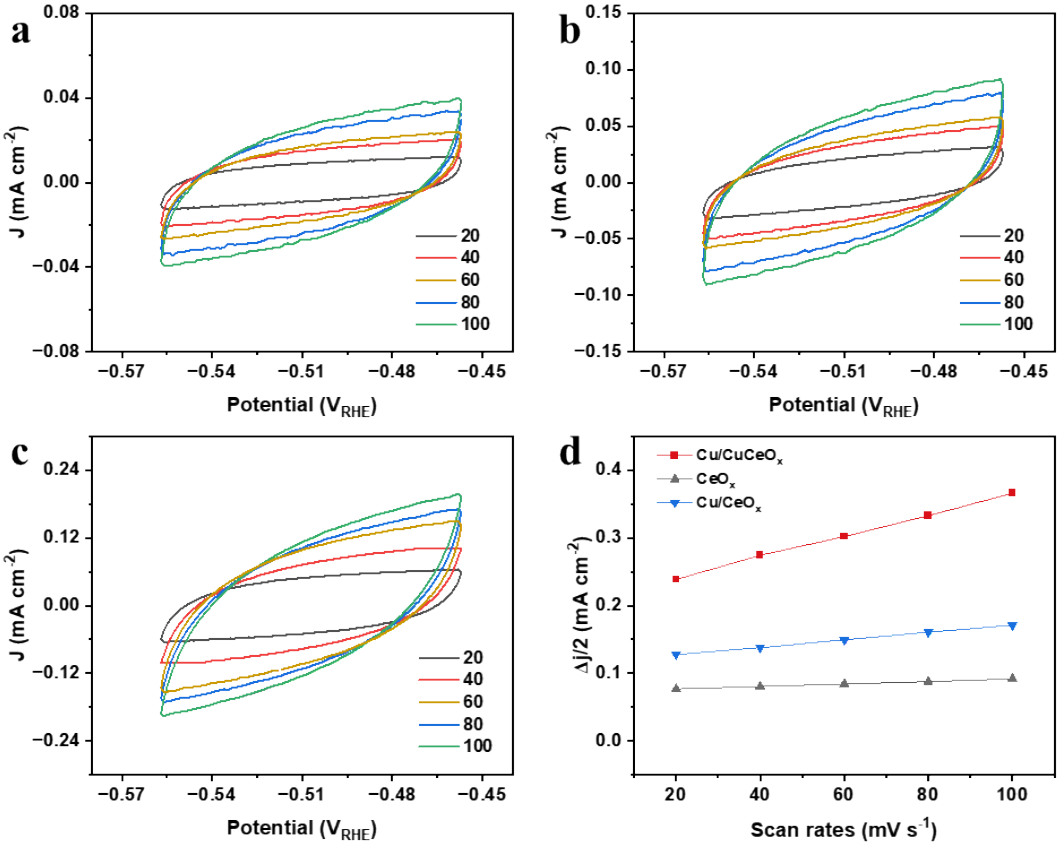

Figure S8 The cyclic voltammogram of (a) CeO_x and (b) Cu/CeO_x (c) $Cu/CuCeO_x$ (d) the corresponding ECSAs of CeO_x, Cu/CeO_x, $Cu/CuCeO_x$.

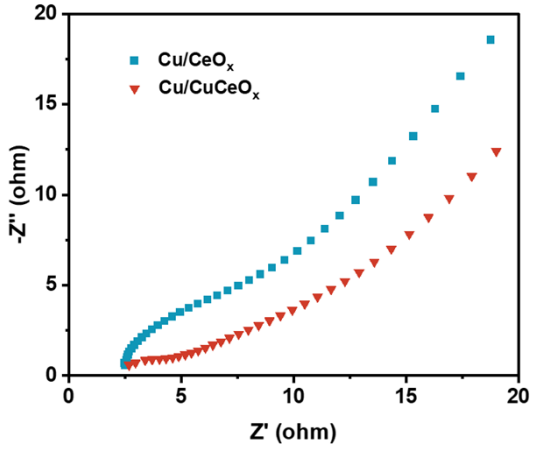

Figure S9 The impedance spectra of Cu/CeO_x and $Cu/CuCeO_x$.

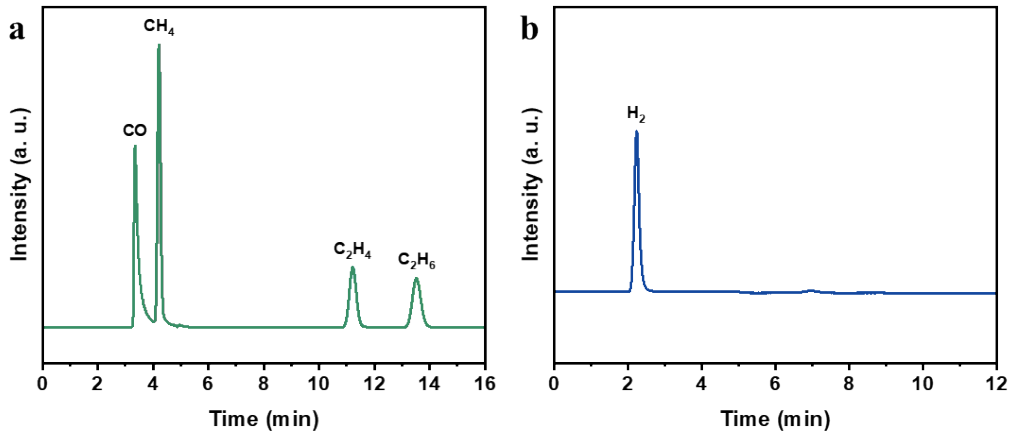

Figure S10 (a) FID and (b) TCD signals detected by GC 2060 of standard gases.

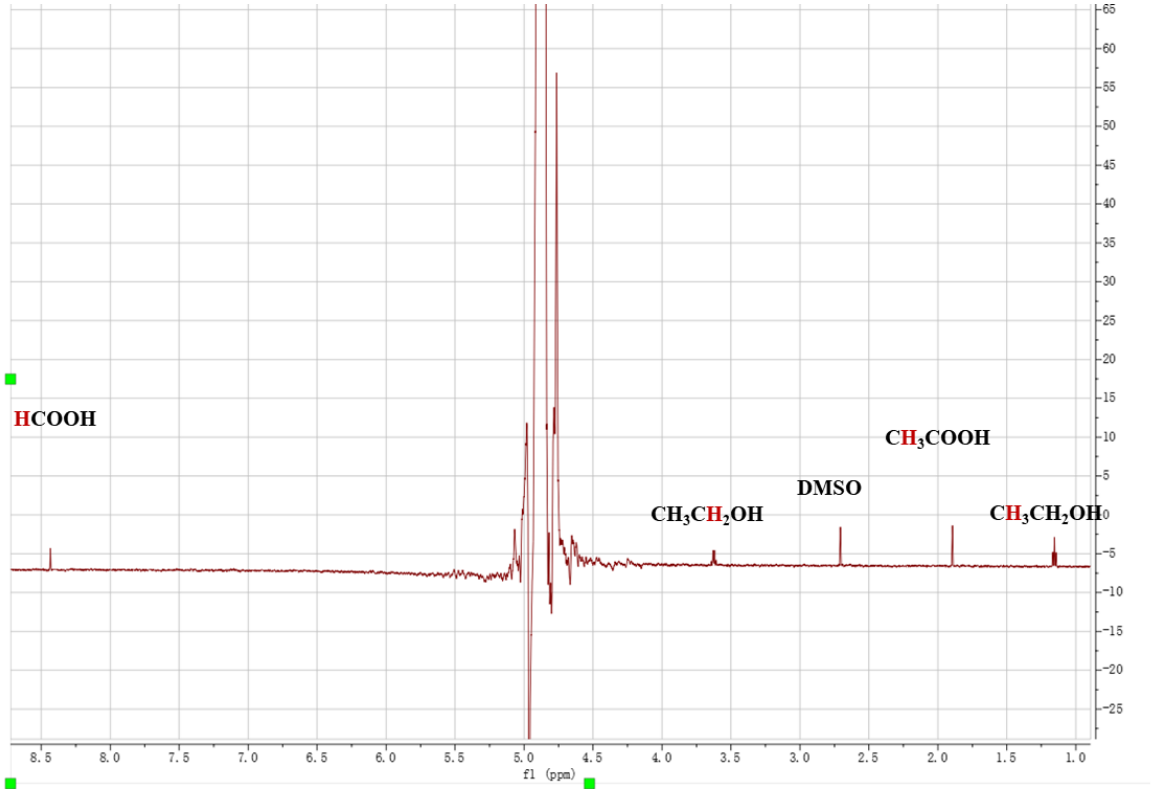

Figure S11 A typical ^{1}H NMR spectrum of the Cu/CuCeO$_x$ catalyzed CO_2 electroreduction at -1.2 V_{RHE}.

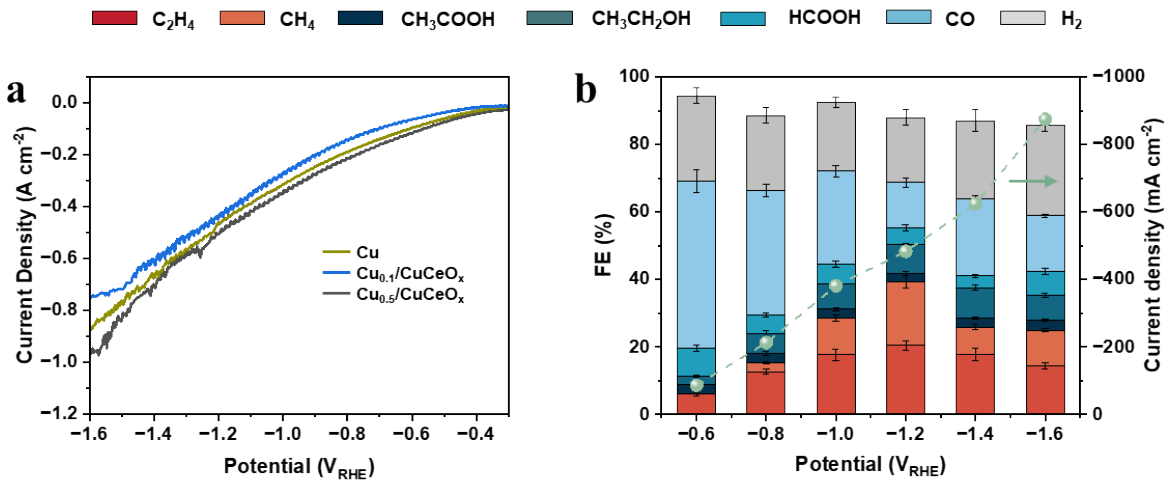

Figure S12 (a) LSV spectra of Cu and $Cu_y/CuCeO_x$ nanorods catalysts. FEs of products at different applied potentials in 1.0 M KOH electrolyte for Cu.

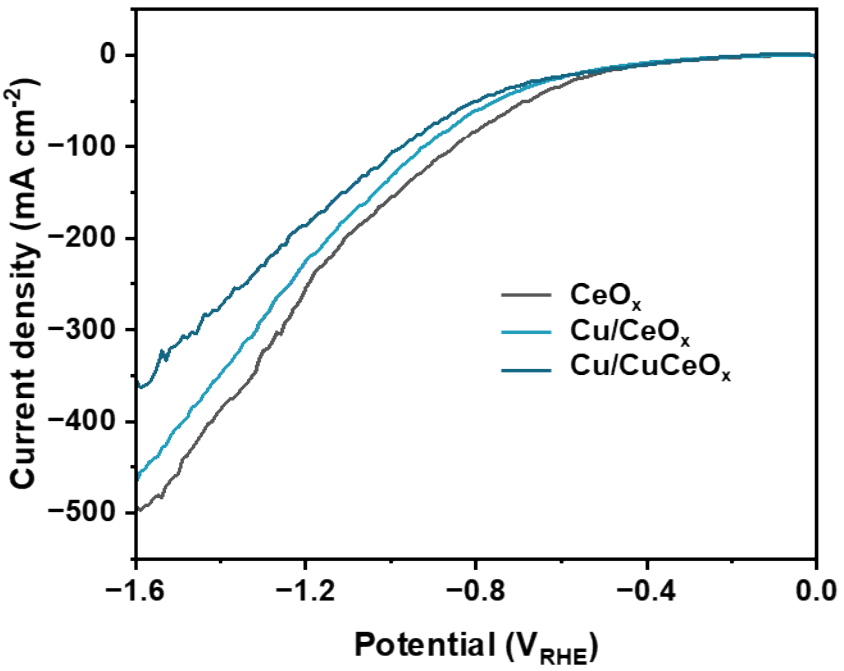

Figure S13 LSV spectra of nanorods catalysts in Ar-saturated 1.0 M KOH electrolytes.

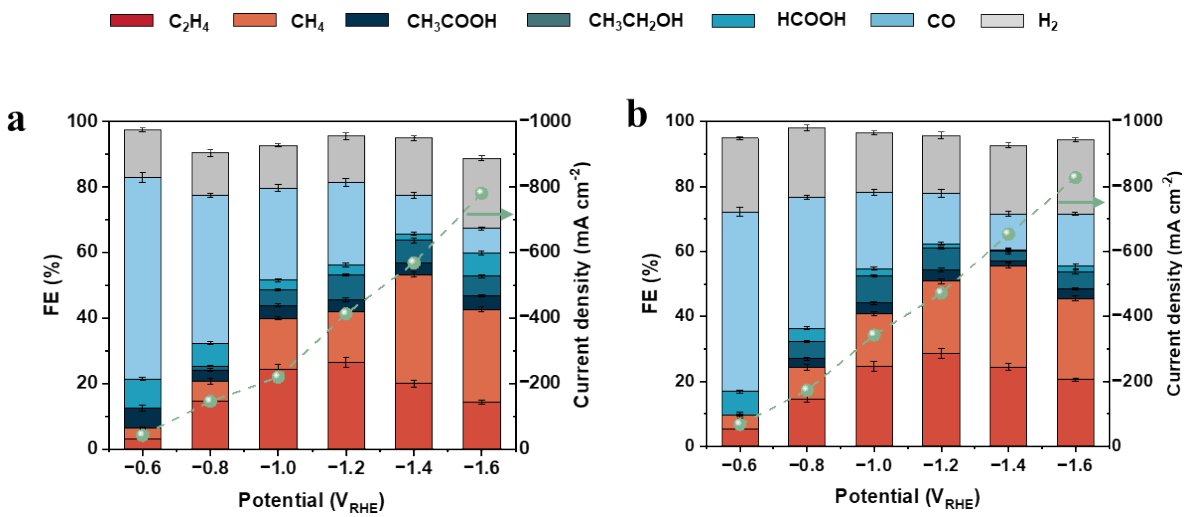

Figure S14 FEs of products at different applied potentials in 1.0 M KOH electrolyte for (a) $Cu_{0.1}/CuCeO_x$, (b) $Cu_{0.5}/CuCeO_x$.

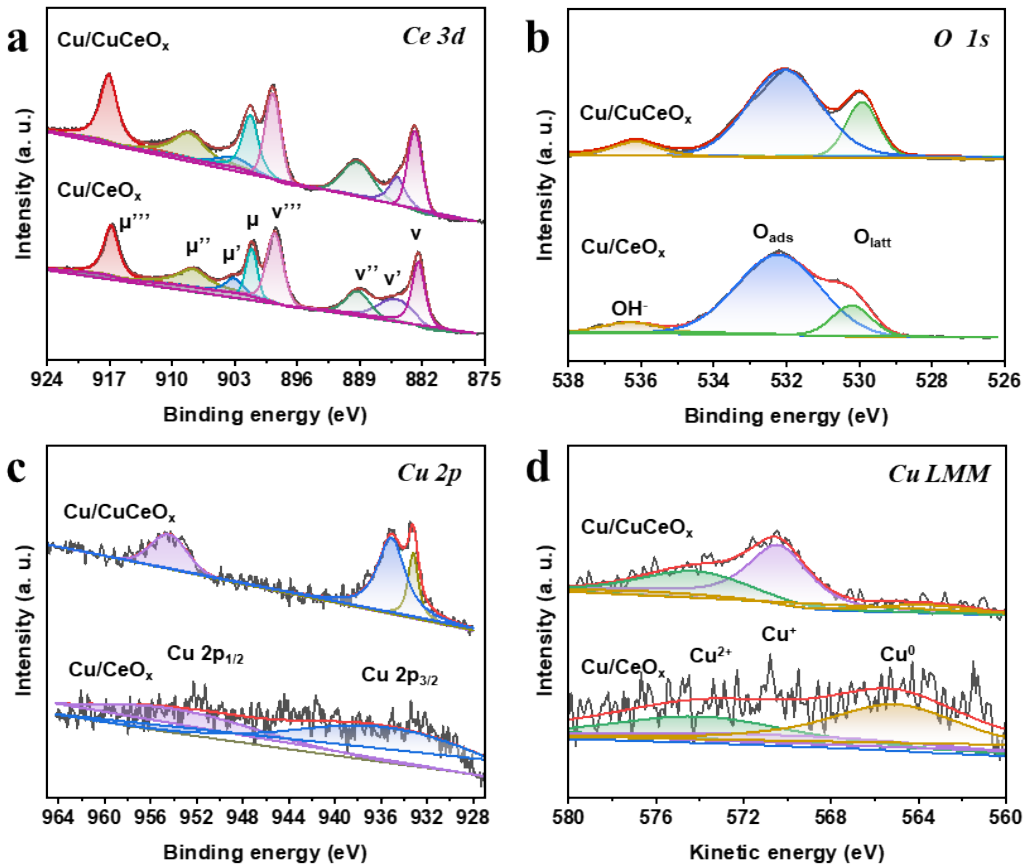

Figure S15 XPS analysis of (a) Ce 3d, (b) O1s, (c) Cu 2p and (d) Cu LMM of $Cu/CuCeO_x$ and $Cu/CuCeO_x$ after CO_2RR.

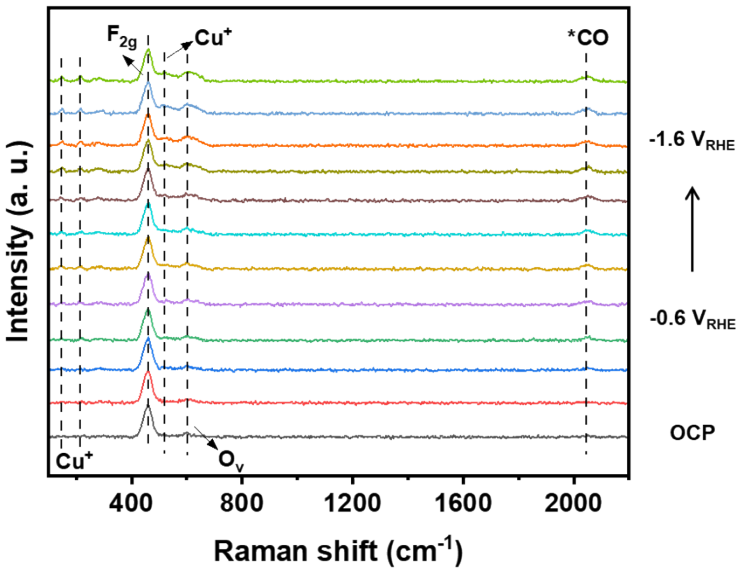

Figure S16 In situ Raman spectra of Cu/CuCeO$_x$ observed in the range of 100 to 2200 cm^{-1} at different applied potentials.

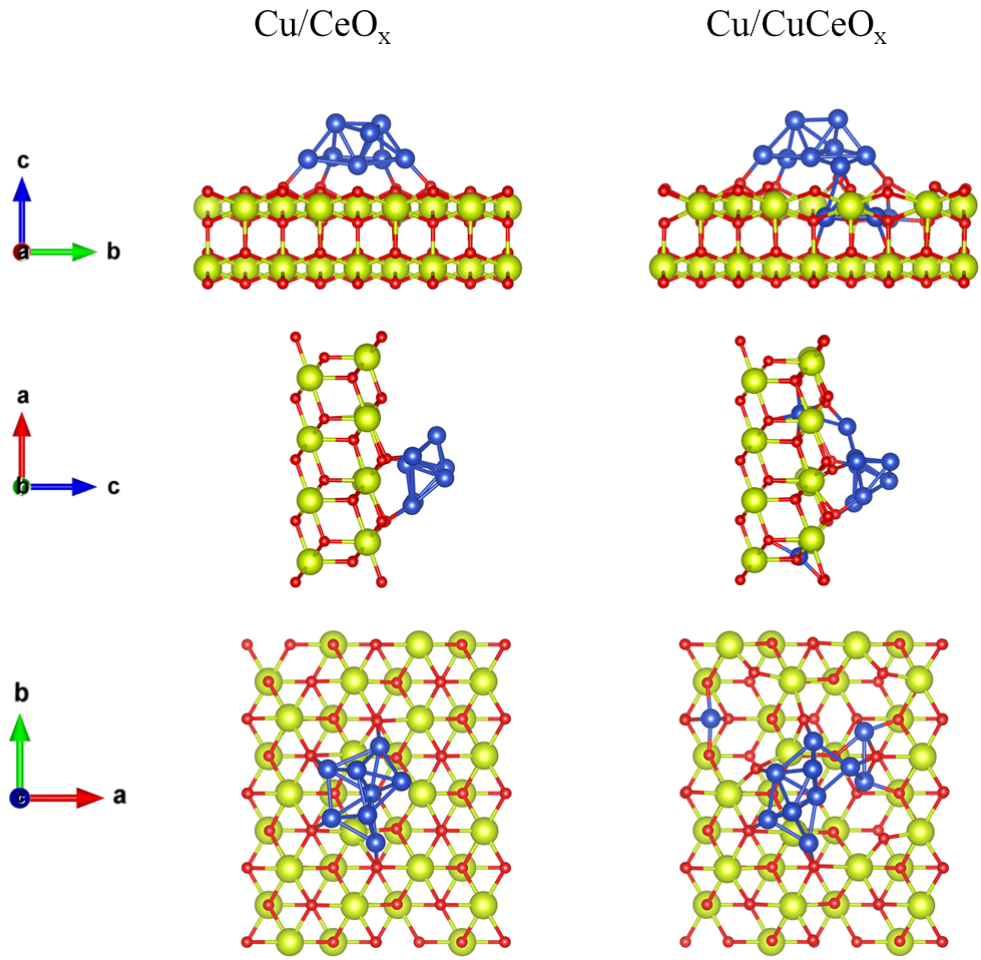

Figure S17 Schematic diagram of Cu/CeO$_x$ and Cu/CuCeO$_x$ cells in different directions. The atoms green, blue and red represent Ce, Cu, and O, respectively.

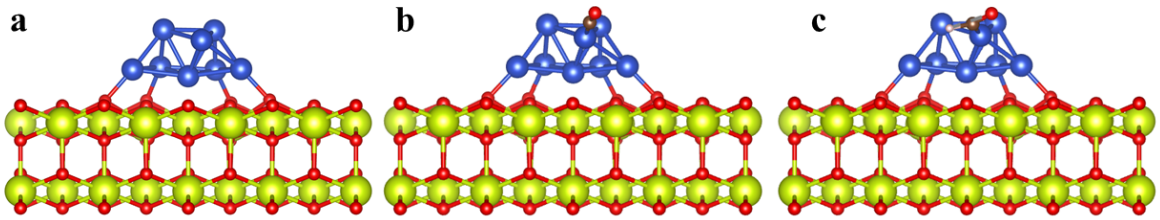

Figure S18 The optimized adsorption configurations of reaction intermediates for C_1 on the Cu/CeO_x (111) structure. (a) Cu/CeO_x, (b) *CO, (c) *CHO. The atoms green, blue, brown, red and white represent Ce, Cu, C, O, and H, respectively.

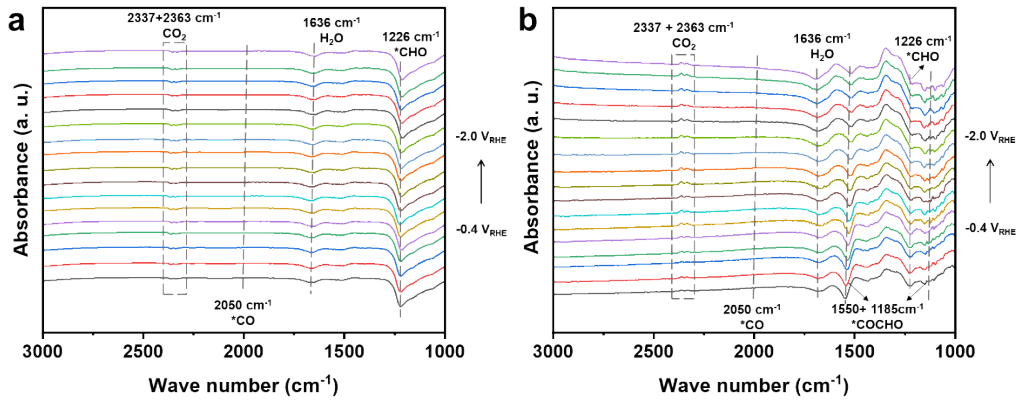

Figure S19 *In-situ FTIR* spectra of (a) Cu/CeO_x and (b) $Cu/CuCeO_x$ catalyst collected at different potentials.

Table S1 Summary of ICP and XPS results.

Sample	Cu/(Cu+Ce)	Ce^{3+}/Ce	OV_s %	$Cu^{+}/Cu^{\delta+}$
CeO_x	/	0.1053	0.152	/
Cu	/	/	/	0.670
Cu/CeO_x	0.288	0.114	0.163	0.561
$Cu_{0.3}/CeO_x$ - CO_2RR	/	0.083	0.132	0.210
$Cu_{0.1}/CuCeO_x$	0.098	0.069	0.161	0.752
$Cu/CuCeO_x$	0.301	0.128	0.293	0.780
$Cu/CuCeO_x$ - CO_2RR	/	0.107	0.241	0.663
$Cu_{0.5}/CuCeO_x$	0.486	0.122	0.166	0.721

The Cu/(Cu+Ce) ratio estimated by ICP analysis; The Ce^{3+}/Ce, OV_s and $Cu^{+}/Cu^{\delta+}$ ratio obtained from the Ce 3d, O1s and Cu LMM XPS result.

Table S2 Ce 3d XPS results. The listed-out figures are the bind energies (BE) and the area of each peak.

peak	Binding Energy (eV)	CeO_x	$Cu_{0.1}/CuCeO_x$	$Cu/CuCeO_x$	$Cu_{0.5}/CuCeO_x$
μ‴	916.6-916.9	150754.5	204966.5	239336.6	20329.41
μ″	907.5-907.7	138632	134444.1	198733.8	11767.9
μ′	903.5-904.2	26110.69	18754.91	52300.69	5268.183
μ	900.6-901	104514.2	217634.5	207280.5	10072.37
ν‴	898.2-898.5	164187.1	212508	248005.1	21848.11
ν″	889.1-889.3	118230.2	196233.8	149727.7	11151.09
ν′	885.1-885.8	69941.7	71772.02	141931.2	9331.582
ν	882.2-882.6	139634.5	252735.7	277080.1	30146.67
	Ce^{4+}	815952.5	1218522.6	1320163.8	105315.55
	Ce^{3+}	96052.39	90526.93	194231.89	14599.765
	Ce^{3+} / Ce^{4+}	0.1177181	0.07429237	0.14712711	0.13862788
	Ce^{3+}/Ce	0.10532	0.06915	0.128257	0.12175

Table S3 O 1s XPS results. The area percent of each deconvoluted peak at different BE are listed. The number of oxygen vacancies is calculated using equation (4).

peak	Binding Energy (eV)	CeO_x	$Cu_{0.1}/CuCeO_x$	$Cu/CuCeO_x$	$Cu_{0.5}/CuCeO_x$
O_{latt}/A_L	528.9–529.2	171016.2	169750.2	28155.22	172466.8
O_{ad}/A_S	530.8–531.3	75048.52	80518.78	39935.29	85642.26
OH^-	533.3–533.6	0	0	0	0
Oxygen vacancy (%)		0.15249752	0.160864483	0.2932515	0.165903

$$Oxygen\ vacany\ (\%) = \frac{1}{2A_s + A_L} \times 100 \quad (4)$$

Catalysts	Electrolyte	Products	FE	FE_{C2H4}/	Potential	$j_{partical}$	Ref.

				FE_{CH4}	(V_{RHE})	(mA cm^{-2})	
Ag_1/CeO_2	[C4mim][BF4] (1.2M)/MeCN	CO	97.2	/	/	403	[6]
Cu/CeO_2@CNF	1.0 M KOH	CO	59.2	/	-0.6	59.2	[7]
Au-CeO_2	0.5 M $KHCO_3$	CO	97	/	-0.6	16	[8]
Cu/CeO_2-R	0.1 M $KHCO_3$	CH_4	49.3	/	-1.6	7.888	[9]
Cu/CeO_2	1.0 KOH	CH_4	67	/	/	364	[10]
Cu/CeO_{2-x}	0.1 M $KHCO_3$	CH_4	54	/	-1.2	/	[11]
Cu/CeO_2	1.0 M KOH	CH_4	42	/	-0.89	51	[12]
Cu-CeO_{2-x}	0.1 M $KHCO_3$	CH_4	58	/	-1.8	70	[13]
Cu/Ce-MOFs Cu/CeO_2	0.1 M $KHCO_3$	CH_4	57.9	/	-1.3	36.635	[14]
Ce-Cu_2O	0.5 M $KHCO_3$	C_2H_4	25	/	-1.3	9.035	[15]
CuO/CeO_2/CB	0.1 M $KHCO_3$	C_2H_4	50	/	-1.1	5.0	[16]
Cu/CeO_2(110)	0.1 M $KHCO_3$	C_2H_4	39.1	/	-1.05	2.5	[17]
Cu/CeO_2	0.1 M $CsHCO_3$	CH_4 C_2H_4	17.4 47.9	2.7528	-1.14 -1.1	/	[18]
5-CuO/CeO_2 60-CuO/CeO_2	0.1 M $KHCO_3$	CH_4 C_2H_4	37.8 44.8	/ /	-1.27 -1.27	8.7 11.8	[19]
Cu−CeO_2 SA Cu−CeO_2 NP	1.0 M KOH	CH_4 C_2H_4	45.5 43.2	0.9494	-0.9 -0.9	80 115	[20]
Cu_y/CeO_2	0.1 M $KHCO_3$	CH_4 C_2H_4	58 42	0.724	-1.3 -1.2	4.35 7.14	[21]
CuO/CeO_2	0.1 M $KHCO_3$	C_2	62.2	/	-1.4	4.5	[22]
$Cu/CuCeO_x$	1.0 M KOH	C_2H_4	40.2	3.77	-1.2	245.66	This work

Table S4 Comparison of CO_2RR between Ce/CeO_2 and other reported catalysts.

Reference

1. X. Guo, W. Ye, Z. a. Chen, A. Zhou, D. Jin and T. Ma, *Appl. Catal. B: Environ.*, 2022, **310**, 121334.
2. G. Kresse and J. Furthmüller, *Comp. Mater. Sci.*, 1996, **6**, 15-50.
3. G. Kresse and J. Furthmüller, *Phys. Rev. B Condens. Matter.*, 1996, **54**, 11169-11186.
4. P. E. Blöchl, *Phys. Rev. B*, 1994, **50**, 17953-17979.
5. J. P. Perdew, K. Burke and M. Ernzerhof, *Phys. Rev. Lett.*, 1996, **77**, 3865-3868.
6. Y. Liang, C. Wu, S. Meng, Z. Lu, R. Zhao, H. Wang, Z. Liu and J. Wang, *ACS Appl. Mater.*, 2023, **15**, 30262-30271.
7. X. Zong, J. Zhang, J. Zhang, W. Luo, A. Züttel and Y. Xiong, *Electrochem. Commun.*, 2020, **114**, 106716.
8. J. Fu, D. Ren, M. Xiao, K. Wang, Y. Deng, D. Luo, J. Zhu, G. Wen, Y. Zheng, Z. Bai, L. Yang and Z. Chen, *ChemSusChem*, 2020, **13**, 6621-6628.
9. L. Xue, C. Zhang, J. Wu, Q.-Y. Fan, Y. Liu, Y. Wu, J. Li, H. Zhang, F. Liu and S. Zeng, *Appl. Catal. B: Environ.*, 2022, **304**, 120951.
10. Y. Jiang, K. Mao, J. Li, D. Duan, J. Li, X. Wang, Y. Zhong, C. Zhang, H. Liu, W. Gong, R. Long and Y. Xiong, *ACS Nano*, 2023, **17**, 2620-2628.
11. S. B. Varandili, J. Huang, E. Oveisi, G. L. De Gregorio, M. Mensi, M. Strach, J. Vavra, C. Gadiyar, A. Bhowmik and R. Buonsanti, *ACS Catal.*, 2019, **9**, 5035-5046.
12. K. K. Patra, Z. Liu, H. Lee, S. Hong, H. Song, H. G. Abbas, Y. Kwon, S. Ringe and J. Oh, *ACS Catal.*, 2022, **12**, 10973-10983.
13. Y. Wang, Z. Chen, P. Han, Y. Du, Z. Gu, X. Xu and G. Zheng, *ACS Catal.*, 2018, **8**, 7113-7119.
14. Q. Deng, Y. Yang, W. Zhao, Z. Tang, K. Yin, Y. Song and Y. Zhang, *J. Colloid and Interf. Sci.*, 2023, **651**, 883-893.
15. Y. Sun, J. Xie, Z. Fu, H. Zhang, Y. Yao, Y. Zhou, X. Wang, S. Wang, X. Gao, Z. Tang, S. Li, X. Wang, K. Nie, Z. Yang and Y.-M. Yan, *ACS Nano*, 2023, **17**, 13974-13984.
16. S. Chu, X. Yan, C. Choi, S. Hong, A. W. Robertson, J. Masa, B. Han, Y. Jung and Z. Sun, *Green Chem.*, 2020, **22**, 6540-6546.
17. X. L. Senlin Chu, Alex W. Robertson, Zhenyu Sun., *Acta Phys. -Chim. Sin.* , 2021, **37**, 2009023.
18. C. W. Lee, S.-J. Shin, H. Jung, D. L. T. Nguyen, S. Y. Lee, W. H. Lee, D. H. Won, M. G. Kim, H.-S. Oh, T. Jang, H. Kim, B. K. Min and Y. J. Hwang, *ACS Energy Lett.*, 2019, **4**, 2241-2248.
19. Y. Zhang, K. Li, M. Chen, J. Wang, J. Liu and Y. Zhang, *ACS Appl. Nano Mater.*, 2020, **3**, 257-263.
20. S. Hong, H. G. Abbas, K. Jang, K. K. Patra, B. Kim, B.-U. Choi, H. Song, K.-S. Lee, P.-P. Choi, S. Ringe and J. Oh, *Adv. Mater.*, 2023, **35**, 2208996.

21. J. Yin, Z. Gao, F. Wei, C. Liu, J. Gong, J. Li, W. Li, L. Xiao, G. Wang, J. Lu and L. Zhuang, *ACS Catal.*, 2022, **12**, 1004-1011.
22. Y. Tian, X. Fei, H. Ning, W. Wang, X. Tan, X. Wang, Z. Ma, Z. Guo and M. Wu, *Front. in Chem.*, 2022, **10**, 915759.